RESEARCH ARTICLE

An Improved Mayfly Algorithm With Shading Detection for MPPT of Photovoltaic Systems

HENGSHAN XU [1], MINGYANG ZHAO[1], FEI XUE[2], XUJUN ZHANG[3], AND LEIJIE SUN[4]
[1]College of Electrical Engineering & New Energy, China Three Gorges University, Yichang 443002, China
[2]Electric Power Research Institute, State Grid Ningxia Electric Power Company Ltd., Yinchuan 750001, China
[3]State Grid Gansu Electric Power Research Institute, Lanzhou 730070, China
[4]XJ Group Corporation, Xuchang 461001, China

Corresponding author: Hengshan Xu (xuhengshan@ctgu.edu.cn)

ABSTRACT A maximum power point tracking (MPPT) method based on improved mayfly algorithm (IMA) with shading detection is proposed to realize the global MPPT with multiple-peak P-V characteristic curve under partial shading condition (PSC) and rapid MPPT with single-peak P-V characteristic curve under uniform irradiance condition (UIC) for photovoltaic array in this paper. Firstly, the characteristic of current-voltage curve in the ideal current source region for photovoltaic array is analyzed, and a shading detection strategy is proposed to monitor the shading condition of photovoltaic array to identify the multi-peak and single-peak on P-V curve. Secondly, the IMA with the elimination strategy is proposed to realize multi-peak MPPT. Meanwhile, the IMA with the bisection searching strategy is utilized to realize quick single-peak MPPT. Finally, simulation and experiment are conducted to verify the effectiveness of the proposed IMA MPPT method, and the results show that the IMA MPPT method can not only identify multi-peak and single-peak effectively, but also improve the tracking efficiency and accuracy in single-peak and multi-peak MPPT scenarios.

INDEX TERMS Maximum power point tracking, shading detection, mayfly algorithm, partial shading condition.

I. INTRODUCTION

Solar energy is a kind of promising renewable energy source, and obtains increasing popularity due to merits of zero-waste production and low costs [1]. Because the voltage of single photovoltaic (PV) module is too low to supply high enough voltage for converter to connect to grid, multiple PV modules are often in series to compose a higher-voltage PV array [2]. Compared with single PV module, it is crucial for large scale PV system to maximize the captured solar energy in different radiation conditions. Consequently, the maximum power point tracking (MPPT) control is widely adopted to improve the energy conversion efficiency of photovoltaic system.

Under uniform irradiance condition (UIC), the power-voltage (P-V) characteristic of the PV system presents one maximum power point (MPP), classical MPPT may adapt to this condition. Among many classical algorithms, hill climbed [3], perturb and observe [4] and incremental conductance [5] are the most common methods. However, due to the shadow of buildings, clouds and dust blocks the PV array, it leads partial shading condition (PSC) to the PV array. And thus, multiple peaks present on the P-V curve of photovoltaic system, with one global maximum power point (GMPP) and multiple local maximum power points (LMPP). In this case, it is difficult for classical MPPT algorithms to find the GMPP, since they can easily get stuck at one of the multiple LMPPs and result in power loss [6].

To accurately search the GMPP under PSC, researchers have resorted to the metaheuristic algorithms, i.e., soft computing method that optimizes the search for the GMPP
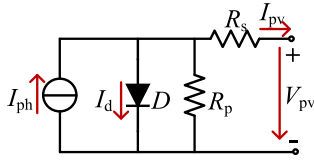
FIGURE 1. Single diode equivalent circuit of a solar cell.

TABLE 1. Specifications of MSX-60.

Variable	Value	Variable	Value
P_{MPP}	60W	R_s	0.35Ω
V_{MPP}	17.1V	R_p	176.4Ω
I_{MPP}	3.5A	K_I	0.003A/°C
V_{oc}	21.1V	K_v	-0.08V/°C
I_{sc}	3.8A	N_s	36

FIGURE 2. Schematic diagram of a 4S1P PV array.

on the P-V curve. And particle swarm optimization (PSO) has the most applications due to its simple structure and excellent optimization capabilities [7]. Literature [8] proposed a MPPT method based on adaptive velocity PSO to improved tracking efficiency by continuously adjusting the weight factor and cognitive acceleration coefficient of particle. In [9], it proposed a GMPPT technique that adopts two PSO algorithms combined with the P&O algorithm to track the MPP at uniform irradiance to avoided unnecessary power oscillations. However, these algorithms for PSCs may suffer from slow or premature convergence. Additionally, recent metaheuristic-based MPPT techniques include differential evolution [10], falcon optimization [11], cuckoo search [12], moth-flame optimization [13], firefly algorithm [14], gray wolf optimization [15], and flower pollination [16], and many others. In principle, above metaheuristic algorithms need to fully scrutinize the searching area (i.e., the P-V curve), before it can converge to the GMPP [17]. However, if metaheuristic algorithms are utilized in no shadow situation, it will result in waste of computing power and lead to longer optimization time, even lower efficiency than conventional algorithms. Another issue is the fluctuations in power caused by the continuous movement of the operating point, which can be generally attributed to the randomness of algorithms in exploration process [18]. Obviously, metaheuristic algorithms are not suitable for rapid single-peak tracking under UIC. Therefore, it is necessary to identify the shading situation of PV array. On this basis, different methods will be adopted under UIC and PSC to ensure tracking benefits.

To realize accurate GMPPT with multiple peaks under PSC and rapid LMPPT with single peak under UIC, a PV MPPT method based on improved mayfly algorithm (IMA) with shading detection is proposed. Mayfly algorithm (MA) is a new heuristic algorithm proposed by K.Zervoudakis and S.Tsafarakis in 2020, which has the advantages of fast convergence speed and global search ability [19], [20]. In this paper, to detect the occurrence of PSCs, variation on current-voltage (I-V) curve under different irradiance conditions is considered. On this basis, a mechanism is designed to identify the shading of PV arrays, and an improved mayfly optimization method has been adopted to design a MPPT combining global and local MPPTs. In GMPPT, the IMA with elimination mechanism is utilized to approach the local convergence interval where GMPP is located, and the IMA with bisection search theorem is adopted to local search to suffer from fast convergence in local area to find MPP. This article is organized as follows: Section II describes PV system
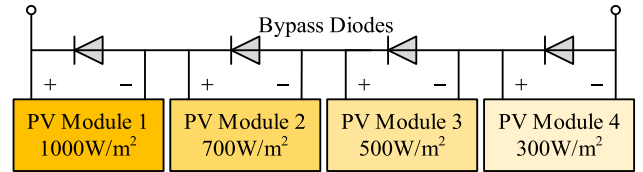
modeling, Section III presents the method based on IMA in detail, Section IV presents simulation results, Section V presents experimental results, and Section VI concludes this article.

II. PV SYSTEM MODELING
A. SINGLE DIODE MODEL
Fig.1 shows the diode equivalent circuit of single solar cell. Multiple cells are connected in series as PV module. V_{pv} is denoted as the terminal voltage of the cell, then the current provided by the cell is

$$I_{pv} = I_{ph} - I_d - \frac{(V_{pv} + I_{pv}R_s)}{R_p} \quad (1)$$

where R_s is the series resistor, R_p is the paralleled resistor, V_{pv} is the output voltage. The photocurrent I_{ph} and the diode dark current I_d are expressed by:

$$I_d = I_0 \left[\exp\left(\frac{q\left(V_{pv} + I_{pv}R_s\right)}{akT} - 1 \right) \right] \quad (2)$$

$$I_0 = \frac{I_{sc\_STC} + K_I \Delta T}{\exp(q(V_{oc\_STC} + K_v \Delta T)/akT) - 1} \quad (3)$$

$$I_{ph} = \frac{G}{G_{STC}}(I_{ph\_STC} + K_I \Delta T) \quad (4)$$

where I_0 is the diode saturation current. a is the diode ideality factor. k is Boltzmann's constant ($1.3806503 \times 10^{-23}$J/K). T is the panel temperature (in standard), q is electron charge ($1.60217646 \times 10^{-19}$ C). G_{STC} and I_{ph_STC} are the radiation and photocurrent at standard test conditions (STC), respectively. V_{oc_STC} and I_{sc_STC} are the open-circuit voltage and short-circuit current at STC, respectively. G is the radiation. K_v and K_I are the temperature coefficients of voltage and current, respectively. ΔT is the temperature difference from STC. In this paper, the solar module MSX-60 is used and the specifications are listed in Tab. 1.

B. OUTPUT CHARACTERISTICS OF PV ARRAY
The classical model of PV array with 4 series and 1 parallel (4S1P) is taken as an example, Fig.2 shows the structure.
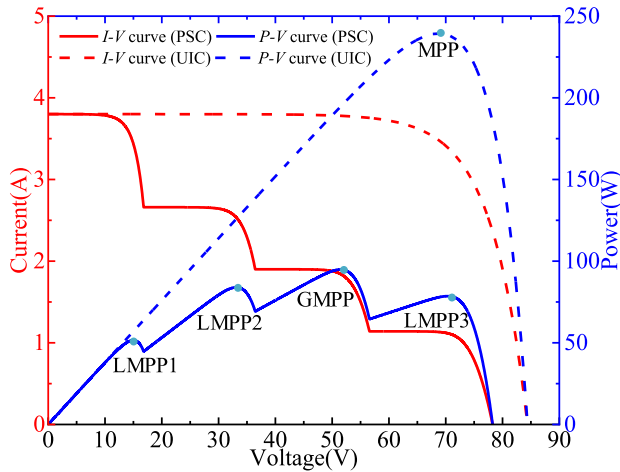
FIGURE 3. I-V and P-V curves of PV array.

A bypass diode is paralleled for each module to prevent the cell from working at reverse voltage.

Fig.3 shows the I-V and P-V curves of this PV array under PSC along with those for an unshaded array. The curves of PV arrays output characteristics under UIC are similar to the superposition of multiple curves of PV modules' output characteristics. Under UIC, the P-V curve has only one MPP. Under PSC, the bypass diode is connected across each module, and the string current is bypassed when the string current is more than the maximum normal current of the shaded module. As a result, a staircase I-V curve is formed, while the corresponding P-V curve generates multiple local peaks. Thus, there is 1 GMPP and 3 LMPPs for P-V curve of 4S1P PV array under PSC.

III. PROPOSED METHOD

A. MAYFLY ALGORITHM
MA simulates the social behavior of mayfly, especially the mating process, which can converge quickly and achieve a good balance between local exploration and global development. In the MPPT algorithm based on MA, the position of each mayfly represents the reference voltage in MPPT control, and the speed represents the change trend of reference voltage. MA aims to change the reference voltage of the PV array through the algorithm mechanism, and compare the output power of the PV array before and after the change to search for the optimal reference voltage value.

Mayfly populations have male individuals and female individuals. Male mayflies gather in groups, and the location of each male mayfly is updated according to its own experience and adjacent individuals. $m_{i,t}$ is denoted as the position of the ith male mayfly in the searching space at time t, and the position is updated by adding the velocity $v_{i,t+1}$ to the current position, then the following relationship can be obtained.

$$m_{i,t+1} = m_{i,t} + v_{i,t+1} \qquad (5)$$

$$v_{i,t+1} = gv_{i,t} + \alpha_1 e^{-\beta r_p^2}(p_{best,i} - m_{i,t}) + \alpha_2 e^{-\beta r_g^2}(g_{best} - m_{i,t}) \qquad (6)$$

where $v_{i,t}$ is the velocity of the ith male mayfly at time t. g is the gravity coefficient. α_1 and α_2 are the positive attraction constants used to scale the contribution of cognitive and social component, respectively. $p_{best,i}$ is the historical optimal reference voltage of the ith male mayfly. g_{best} is the global optimal reference voltage among male mayflies. β is a fixed visibility coefficient. r_p is the Cartesian distance between m_i and $p_{best,i}$. r_g is the Cartesian distance between m_i and g_{best}.

The best individual in the group continues to perform its unique up-and-down moving. Thus, the best male mayfly constantly changes its velocity. The velocity can be expressed as

$$v_{i,t+1} = v_{i,t} + dr \qquad (7)$$

where d is the nuptial dance coefficient and r is a random value in the range $[-1, 1]$.

Female mayflies move toward male mayflies to reproduce. If $f_{i,t}$ is the position of the ith female mayfly at time t, then the position $f_{i,t+1}$ of the ith female mayfly at time $t + 1$ is

$$f_{i,t+1} = f_{i,t} + v_{i,t+1} \qquad (8)$$

The velocity of female mayfly depends on the behavior of male mayfly. To maximize the output power, the velocity $v_{i,t+1}$ of the ith female mayfly is updated by

$$v_{i,t+1} = \begin{cases} gv_{i,t} + \alpha_2 e^{-\beta r_{mf}^2}(m_{i,t} - f_{i,t}) & P(f_{i,t}) < P(m_{i,t}) \\ gv_{i,t} + \lambda r & P(f_{i,t}) \geq P(m_{i,t}) \end{cases} \qquad (9)$$

where r_{mf} is the Cartesian distance between m_i and f_i. λ is a random walking coefficient. $P(\cdot)$ is the output power that the mayfly represents. If the female is not interested in the male, the male will move randomly.

The mating process between two mayflies is as follows: one parent is selected from the male population, and another parent is selected from the female population. Two offspring are generated from two parents and given by

$$\begin{cases} m_{offspring1} = Lm + (1-L)f \\ m_{offspring2} = Lf + (1-L)m \end{cases} \qquad (10)$$

where m is the male parent, f is the female parent and L is a random value within $[0, 1]$.

B. DESIGN OF SHADING DETECTION MECHANISM
To judge the irradiance of PV array, a shadow detection mechanism is proposed. As shown in Fig.3, without shadow, the irradiance of each PV module is 1000 W/m², when the output voltage V_{PV} of PV array varies within $[0, V_{mpp}]$, the output current I_{PV} of PV array is almost not changed. In this area, the PV array can be seen as an ideal current source, called quasi-ideal current source area. However, under PSC, when V_{PV} varies within $[0, V_{mpp4}]$, I_{PV} decreases by a step. Therefore, the output current of PV array will be greatly affected by the irradiance under PSC, and whether PSC happens can be reflected by the change rate of the output current. When one generation of mayflies finish the calculation and
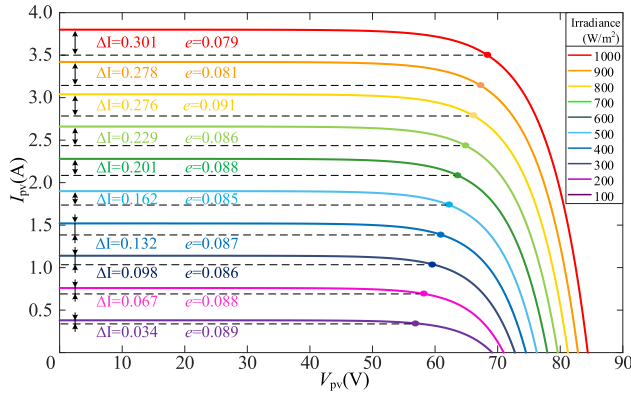
FIGURE 4. I-V curves under uniform irradiance intensity.

output the value, the current that every mayfly represents will be sampled. The change rate of current can be calculated by

$$\varepsilon = \frac{|I_{\max} - I_{\min}|}{I_{\max}} \quad (11)$$

where $I_{\max}$ and $I_{\min}$ are the maximum and minimum output current values of the PV array in the population of mayflies in algorithm, respectively. If ε is less than the threshold value, PV array is working without shadow. Otherwise, PV array is working under PSC.

To properly design the threshold, all the irradiance conditions should be considered. In this paper, a series of I-V characteristics for different irradiance of 4S1P PV array in Fig.2 are simulated, and then the threshold is selected with considering the above series I-V characteristics. Fig.4 shows the I-V characteristic curves of PV array for different uniform irradiance intensity within [100, 1000] W/m², and ΔI is the current difference between I_{sc} and I_{mpp}. As shown in Fig.4, each ΔI is less than the current difference caused by irradiance changing 100W/m². Compared with the occurrence under PSC, however, the impact on P-V curve caused by variation of irradiance around 100W/m² is negligible. In quasi-ideal current source region, the maximum current change rate can be calculated by $e = \Delta I / I_{sc}$. The threshold should be designed as a higher value than e to cover the effect of all the irradiance on the P-V characteristic, as Fig.4 shows, the threshold $\varepsilon_{\max} = 0.1$ is enough to cover all the irradiance, in this case, there is even some margin left.

Assuming that the number of PV modules in series in an array is n, the P-V curve will generate n numbers of peaks under PSC at most. V_{oc_mod} is denoted as the open voltage of PV module, and V_{oc_array} is denoted as the open circuit voltages of PV array. When using IMA for global searching, the number of mayflies is n. The position of $mayfly\_i$ $(i = 1, 2, 3, \ldots, n)$ represents a reference voltage of the PV array, and the reference voltage are in $0 \sim V_{oc\_array}$. To fast search the MPP, the initial positions of mayflies are set near $0.8 \times V_{oc\_mod}$. Moreover, to avoid the effect of the initial positions of mayflies on shading detection, the initial position of each mayfly is located at the quasi-ideal current

source area of the output characteristics of PV array, which is set as

$$mayfly\_n = \begin{cases} 0.7V_{oc\_mod} & n = 1 \\ 0.7V_{oc\_mod} + 0.8(n-1)V_{oc\_mod} & n \neq 1 \end{cases} \quad (12)$$

After completing output of one generation of reference voltage represented by positions of mayflies, the rate of change in the sampled PV array current is calculated by (11) to identify the scenarios of irradiance, satisfying the following formula.

$$\varepsilon \leq \varepsilon_{\max}$$
$$\Rightarrow \text{single-peak} P - V \text{curve}$$
$$\varepsilon > \varepsilon_{\max}$$
$$\Rightarrow \text{multi-peaks} P - V \text{curve} \quad (13)$$

When the shading detection is completed, GMPPT is used if the monitoring result is multi-peaks P-V curve, and LMPPT is utilized if the monitoring result is single-peak P-V curve.

C. GMPPT

With MA searching GMPP, because the population number of mayflies increases with the iterations increases, the searching cycle will increase accordingly, which reduces the convergence speed. To solve the above problem, an elimination mechanism is introduced into the proposed IMA. With the elimination mechanism, the size of population is fixed, and the convergence speed is stable. The elimination mechanism is as follows:

$$\begin{cases} mayfly_{k+1}i = mayfly_k i & P(m_{offspring}) \leq P(mayfly_{k\_worst}) \\ mayfly_{k+1}i = m_{offspring} & P(m_{offspring}) > P(mayfly_{k\_worst}) \end{cases} \quad (14)$$

where k is the number of iterations and $mayfly_{k\_worst}$ is the worst individual in the parent population. If the fitness of the offspring generated by (10) is better than that of the parent, the worst parent mayflies will be eliminated and the position will be replaced by the position of the offspring mayflies. Otherwise, the offspring mayflies will be eliminated.

If there are no adjacent individuals around a mayfly in the population, the overall rate of convergence will be slowed down. To solve this problem, the Lévy airplane mode is introduced for the individual, and its step size meets a Lévy distribution, that is

$$\text{Levy}(x) = 0.01 \frac{r_1 \sigma}{|r_2|^{\frac{1}{\beta}}} \quad (15)$$

$$\alpha = \left(\frac{\Gamma(1+\beta) \sin \frac{\pi\beta}{2}}{\Gamma(\frac{1+\beta}{2})\beta \cdot 2^{(\frac{\beta-1}{2})}} \right) \quad (16)$$

where r_1 and r_2 are both random numbers between 0 and 1, β is a constant, taken as 1.5 in this article, and $\Gamma()$ is a common gamma function in mathematics.
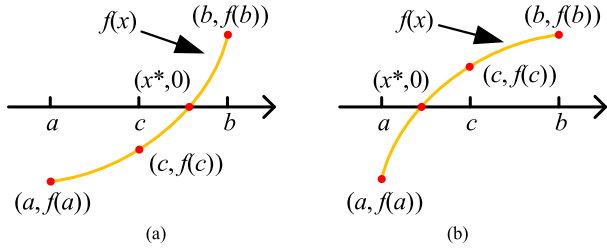
FIGURE 5. Process for bisection search in: (a) case 1, (b) case 2.

FIGURE 6. Principle for bisection search in MPPT.

In the absence of any adjacent individuals, the individual position of the $(t + 1)$ generation of mayfly population is updated as follow:

$$X_{t+1} = X_t + \text{Levy}(x)X_t \qquad (17)$$

The MPP searching of photovoltaic system is similar to the movement of population in low density area. The introduction of Lévy airplane mode to the mayfly without adjacent individuals can increase the probability of successful searching. In addition, it can prevent the mayfly without adjacent individuals from moving too slowly, speed up the rate of convergence of the algorithm, and improve the dynamic tracking performance of the algorithm.

In the process of GMPPT, if the output current of the PV array meets the conditions of single-peak P-V curve, the proposed IMA will switch to LMPPT.

D. LMPPT

The MPPT under PSC in local convergence region and MPPT under UIC are single power peak searching problem, and the algorithm switches to LMPPT in this scenario. The binary search strategy is added into the LMPPT to fast locate the MPP. Fig.5 shows the diagram of the binary search strategy. If the root x^* of the function $f(x)$ is within $[a, b]$, the searching interval is repeatedly divided be binary search strategy with the initial midpoint c to close the x^*, where $c = (a + b)/2$.

The root of the function $f(x)$ has three cases, including:

Case 1: If $f(b)f(c) < 0$, $x*$ is within $[c, b]$, as shown in Fig.5(a).

Case 2: If $f(a)f(c) < 0$, x^* is within $[a, c]$, as shown in Fig.5(b).

Case 3: If $f(c) = 0$, $x^* = c$.

ΔP is the power variation, and the ΔP near MPP is close to 0. The target function $y = f_{\Delta P}$ of MPPT based on binary search strategy is a function of V_{PV}, that is

$$y = f_{\Delta P}(V_{\text{pv}}) \qquad (18)$$

Supposing $V_{a,j}$ is the left end point of the interval and $V_{b,j}$ is the right end point of the interval in the bisection search theorem, where j is the number of searches. When enter the local search, the positions of the two mayflies with the farthest distance between the current positions are taken as the endpoints of the first interval of the bisection search,
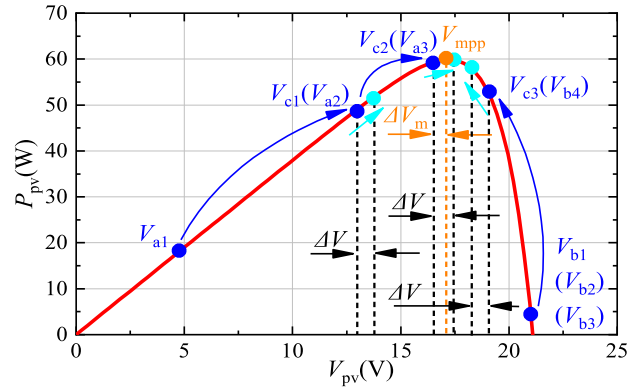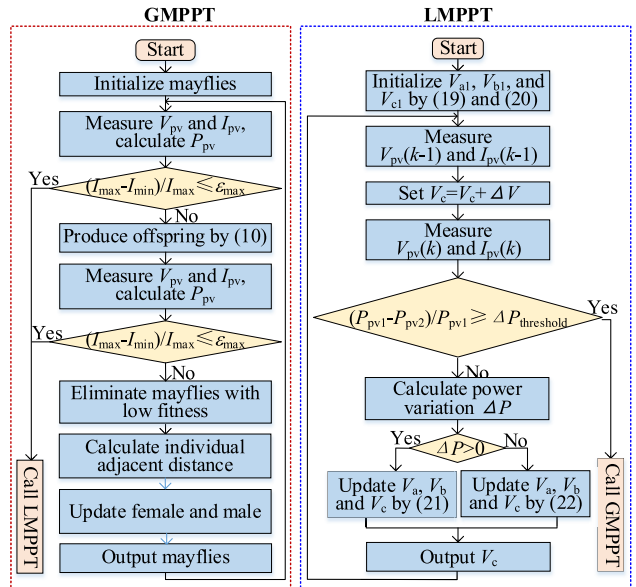

FIGURE 7. Flowchart of the proposed IMA.

which are expressed by the following formula:

$$\begin{cases} V_{a,1} = \min(mayfly\_i) \\ V_{b,1} = \max(mayfly\_i) \end{cases} \qquad (19)$$

And the voltage at the midpoint of the interval is

$$V_{c,j} = \frac{(V_{a,j} + V_{b,j})}{2} (j = 1, 2, 3, \ldots, n) \qquad (20)$$

The power at $V_{c,j}$ is P_1, and a voltage increment ΔV is superimposed on $V_{c,j}$ to obtain a power P_2, and the power difference between $V_{c,j}$ and $V_{c,j} + \Delta V$ is $\Delta P = P_2 - P_1$. When $\Delta P > 0$, the search interval of the reference voltage is updated according to the following equation:

$$\begin{cases} V_{a,j+1} = V_{c,j} \\ V_{b,j+1} = V_{b,j} \\ V_{c,j+1} = (V_{c,j} + V_{b,j+1})/2 \end{cases} \qquad (21)$$
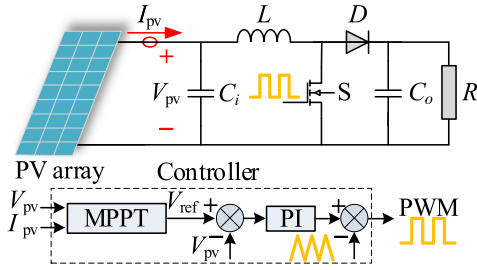
FIGURE 8. Schematic of boost DC/DC converter structure.

TABLE 2. Irradiance of PV modules.

	Radiation(W/m²)			
	Module1	Module2	Module3	Module4
UIC	1000	1000	1000	1000
PSC	1000	700	500	300

When $\Delta P < 0$, the search interval of the reference voltage is updated according to the following equation:

$$\begin{cases} V_{a,j+1} = V_{a,j} \\ V_{b,j+1} = V_{c,j} \\ V_{c,j+1} = (V_{a,j+1} + V_{c,j})/2 \end{cases} \tag{22}$$

The above searching process is presented in Fig.6. On the one hand, as the iteration increases, $V_{c,j}$ is gradual close to V_{mpp}. On the other hand, as the distance between $V_{c,j}$ and V_{mpp} decreases, if $\Delta V_m < \Delta V$, $V_{c,j} + \Delta V$ not only steps over V_{mpp} at the present iteration, but also steps over V_{mpp} at the next iteration, leading the reference voltage to fluctuates near V_{mpp}. To reduce the power fluctuation in the above case, the reference voltage can be set as the historical optimal value. Therefore, the reference voltage keeps the existed optimal output when the searching interval is shorter that 1% V_{oc_array}, because ΔP is close to 0 near MPP.

E. RESTART CONDITIONS AND FLOWCHART

After the PV system is stable, the P-V curve of the array will be changed if the variation of irradiance, and the system will no longer operate at the maximum power point. When a minor variation occurs to the irradiance intensity, LMPPT can track MPP and stabilize near it. However, a sharp irradiance changes leads to the large-amplitude deviation of MPP, and the algorithm needs to be restarted. If the condition in (23) is satisfied, the system will re-enter GMPPT.

$$\frac{P_{pv1} - P_{pv2}}{P_{pv1}} > \Delta P_{threshold} \tag{23}$$

where P_{pv1} and P_{pv2} are the power sampling values of PV array before and after the power changing respectively, and ΔP_{th} is the threshold value of power change caused by sharp irradiance change, which is determined by the power of the main circuit [21]. The flow chart of the whole IMA is shown in Fig.7.

TABLE 3. Convergence time for different *g*.

α_1	α_2	g	Convergence time
1	1.5	0.4	0.38s
1	1.5	0.6	0.37s
1	1.5	0.8	0.36s
1	1.5	1.0	0.45s
1	1.5	1.2	0.48s

TABLE 4. Convergence time for different α_1.

α_1	α_2	g	Convergence time
1.2	1.5	0.8	0.36s
1.4	1.5	0.8	0.36s
1.6	1.5	0.8	0.36s
1.8	1.5	0.8	0.36s
2.0	1.5	0.8	0.36s

TABLE 5. Convergence time for different α_2.

α_1	α_2	g	Convergence time
1	1.6	0.4	0.36s
1	1.7	0.6	0.36s
1	1.8	0.8	0.36s
1	1.9	1.0	0.36s
1	2.0	1.2	0.36s

IV. SIMULATIONS RESULTS

To evaluate the performance of the proposed method, the simulation model of PV system as shown in Fig.8 is built. In simulation, the PV system consists of PV array, boost circuit, resistance load and controller. The simulation parameters are in consistent with Tab. 1, and $C_i = 10 \mu F$, $C_o = 50 \mu F$, $L = 1100 \mu H$, $R = 120\Omega$.

The controller includes a MPPT module and a PI modulation module. V_{pv} and I_{pv} are the input signals of MPPT module. The output signal of MPPT module is reference voltage, and the difference between the reference voltage and the actual voltage signal of PV array is modulated by PI module to generate a modulating signal. The pulse width modulated (PWM) signal is generated by comparing the triangular carrier signal with the modulating signal. The PWM signal can control MOSFET to regulate the output of PV system. The proportional coefficient K_p and integrator coefficient K_i are set as 20 and 5, respectively. In simulation, the sample time of algorithms $T_s = 10ms$ and a switching frequency $f_s = 50kHz$.

The simulations of PSO algorithm and the proposed IMA for MPPT under UIC and PSC are conducted. The irradiances for each PV module are given in Tab. 2. To obtain fair comparation results, the simulation parameters for PSO algorithm and the proposed IMA algorithms are set as the same. The population number is 4. The positions are initialized according to (12). Moreover, the extra parameters of PSO algorithm are set as follows: ω_{max}=0.9, ω_{min}=0.4, c_1=c_2=1.5.

A. EFFECT OF IMA PARAMETERS AND PARAMETERS SELECTION

In the process of IMA for MPP searching, the algorithm parameters are of great significance to the optimization effect. GMPPT is responsible for global fast search. Therefore,
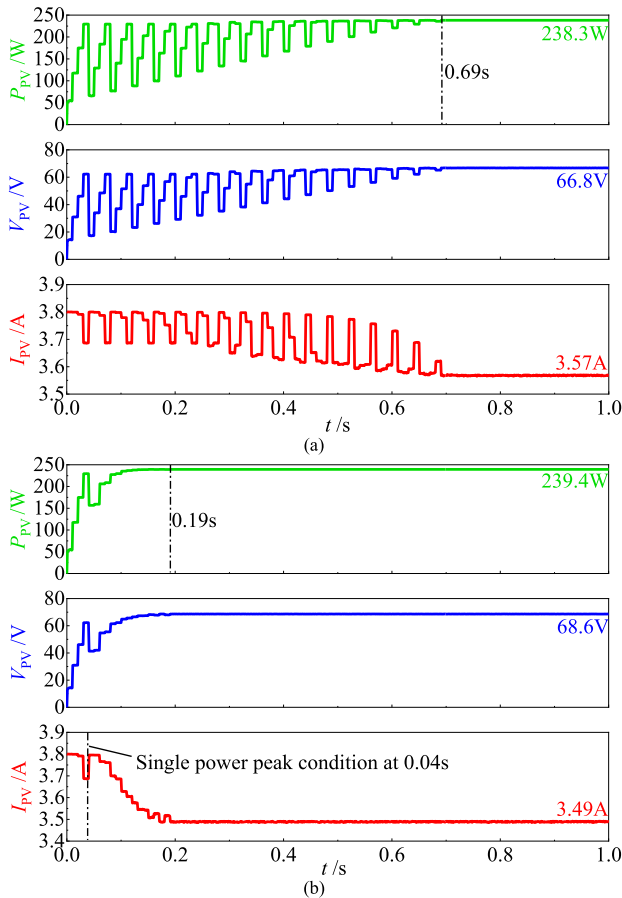
FIGURE 9. Simulation results under UIC with: (a) PSO, (b) IMA.

FIGURE 10. Simulation results under PSC with: (a) PSO, (b) IMA.

under the PSC in Table 2, the effect of GMPPT algorithm parameters on convergence speed is analyzed by simulation experiments. The value range of parameters is shown in [20]. According to the reference voltage value ranging from 0 to V_{oc_array}, the optimization range of mayfly is set within [0, 84.4]. To prevent that the voltage variation of the PV system during the tracking process is too large, the maximum speed of mayfly is set to 5. In the IMA, g, α_1 and α_2 may affect the convergence speed of the algorithm, and the impact on the convergence time of the current system is partly shown in Table 3, Table 4 and Table 5.

The reasons for the above phenomenon are as follows: g inherits some speed information of the last generation, which means that g makes the speed in present generation have relationship with the speed in last generation. α_1 and α_2 has great influence on the optimal moving trend of individuals, but has little influence on the moving speed. Based on the parameters shown in literature [20] and the test results, $g = 0.8$, $\alpha_1 = \alpha_2 = 1.5$, $\beta = 2$, $d = 5$, $\lambda = 1$ in this paper.

B. SIMULATION RESULTS UNDER UIC

Under UIC, the P-V curve obtained with this irradiance is a single peak curve, as shown by the dashed line in Fig.3. And $V_{MPP} = 68.4V$, $I_{MPP} = 3.5A$, $P_{max} = 240W$. Fig.9 shows the
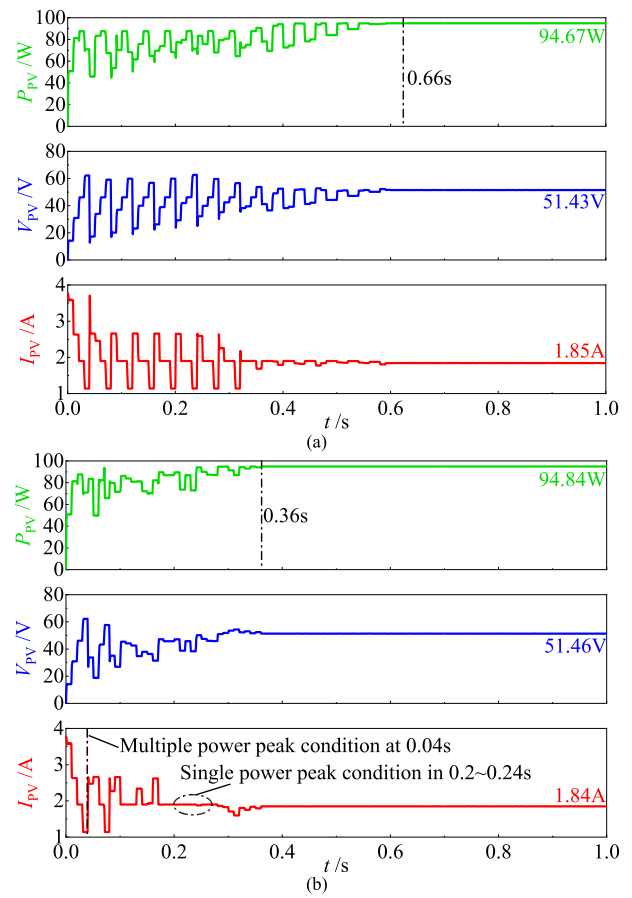
comparison of performance between PSO algorithm and the proposed IMA under UIC.

Under UIC, PSO algorithm keeps the random search in the region, and the convergence time is about 0.69s. And the average power value tracked by PSO algorithm is 238.3W. Assuming the ratio of the average power value tracked to the theoretical maximum power value in the current environment as its tracking accuracy, the tracking accuracy of PSO algorithm is 99.29%. Compared with PSO algorithm, the proposed IMA detects the shadow for 0.04s at the beginning of the algorithm and judges it as a single peak P-V curve since the change rate of current satisfies the conditions of single-peak curve in (12). Then the algorithm switches to the local search method, which reduces the search space through the bisection search theorem, to rapidly locates the peak. The convergence time of IMA is about 0.19s, which is 27.5% of the tracking time of PSO algorithm. The average power value tracked by IMA is 239.4W, and the tracking accuracy of IMA is 99.81%. Further, MPPT technique based on IMA has an advantage over MPPT methods based on PSO algorithm such as fewer power oscillations during transient part of MPPT in uniform irradiance conditions, and the necessity of shading detection is proved, as discussed in Section III.

TABLE 6. Energy and efficiency of PV array.

Items	PSO	IMA	PSO	IMA
Conditions	UIC		PSC	
E_m /W·s	240.0		94.9	
E /W·s	211.1	232.5	88.2	90.5
η	88.0%	96.9%	92.9%	95.4%
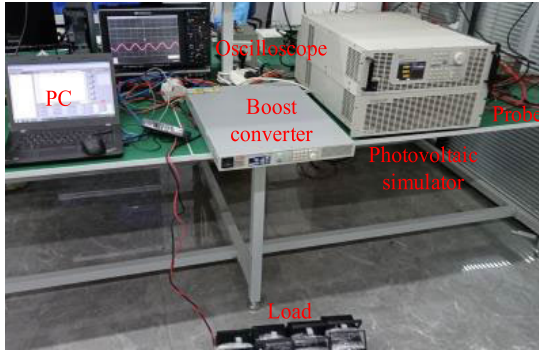
FIGURE 11. Experimental platform of MPPT control system.

FIGURE 12. Measured dynamic waveforms of I_{PV}, V_{PV}, and P_{PV} for: (a) PSO, and (b) IMA.

C. SIMULATION RESULTS UNDER PSC

Under PSC, the P-V curve obtained with this irradiance is a multiple peak curve, as shown by the solid line in Fig.3. And $V_{MPP} = 51.5V$, $I_{MPP} = 1.84A$, $P_{max} = 94.86W$. Fig.10 shows the comparison of performance between PSO algorithm and the proposed IMA under PSC.

From simulation results in Fig.10, the convergence time of PSO algorithm is about 0.66s. The average power value tracked by PSO algorithm is 94.67W, and the tracking accuracy of PSO algorithm is 99.80%. However, the power wave based on PSO algorithm fluctuates around the optimal value within 0.3~0.5s, which causing energy loss. IMA detects the
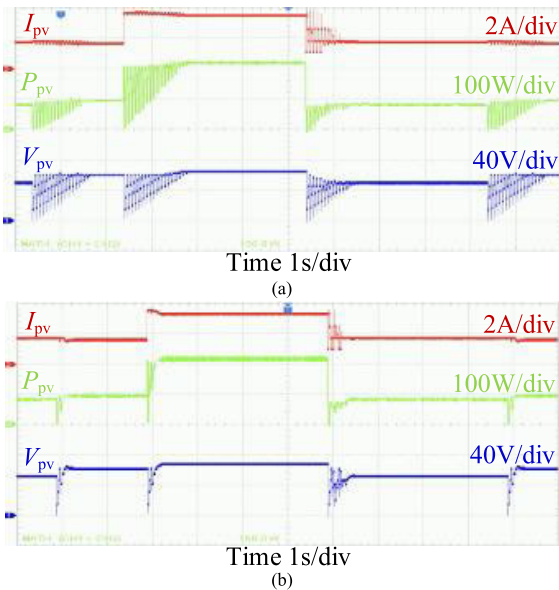

FIGURE 13. Measured waveforms of I_{PV}, V_{PV}, and P_{PV} switching from UIC to PSC for: (a) PSO, and (b) IMA.

shadow for 0.04s at the beginning of the algorithm and judges it as a multi-peak P-V curve, since the change rate of current satisfies the conditions of multi-peaks curve in (12). When the local conditions are satisfied, the proposed method switch GMPPT to LMPPT. The convergence time of IMA is about 0.36s, which is 54.5% of the tracking time of PSO algorithm. The average power value tracked by IMA is 94.84W, and the tracking accuracy of IMA is 99.98%. Moreover, IMA also has fewer power oscillations during transient part of MPPT than that of PSO algorithm under PSC to improve the power generation efficiency of the PV array.

D. EFFICIENCY ANALYSIS

In the process of tracking the MPP through algorithms, the output voltage of the PV system fluctuates randomly. The fluctuation of voltage has an impact on the power quality of PV system. From the waveforms of the output voltage of the PV system under UIC in Fig.9, it can be seen that the output voltage of system adopting the PSO-based MPPT has a large fluctuation amplitude. and the fluctuation is relatively stable at 0.6s. The output voltage fluctuation of system based on IMA is relatively small, and can be stable at 0.1s. From the output voltage waveforms of the PV system under PSC in Fig.10, similarly, the output voltage of system adopting the PSO-based MPPT still has a large fluctuation amplitude, and the fluctuation is relatively stable at 0.6s. The output voltage fluctuation of system based on IMA is relatively small, and can be stable at 0.3s. Overall, the proposed IMA-based MPPT can reduce the amplitude of output voltage fluctuations, stabilize the voltage faster, and have good power quality.

To further explore the impact of power oscillation on photovoltaic power generation during the tracking process, the
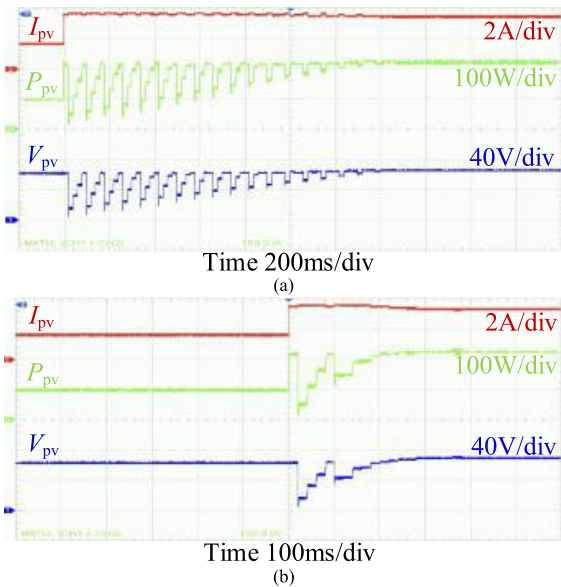
FIGURE 14. Measured waveforms of I_{PV}, V_{PV}, and P_{PV} switching from PSC to UIC for: (a) PSO, and (b) IMA.

power curves in Fig.9 and Fig.10 are integrated to obtain their power generation E during the corresponding time period, and the efficiency η can be calculated by $\eta = E/E_m$, where E_m is the theoretical maximum energy of the PV array under the current operating conditions. The efficiency based on simulation for MPPT methods based on PSO algorithm and IMA are given in Tab. 6. The data about the efficiency are obtained by averaging the multiple sampling results. Under UIC, the efficiency of IMA is higher 8.9% than that of PSO algorithm. Under PSC, the efficiency of IMA is higher 2.5% than that of PSO algorithm. The simulation results in Tab. 4 verify that the performance in efficiency of the proposed IMA-based MPPT method is better than that PSO-based MPPT method under UIC and PSC.

V. SIMULATIONS RESULTS

An experimental platform as shown in Fig.11 is developed to further verify the performance of the proposed IMA MPPT method. The experimental parameters are set as the same with the simulation parameters. The controller is implemented by TMS320 F28335 digital signal processor. And the sampling time of the control system is 20ms.

The restart condition in (23) is adopted by the experiment with PSO-based MPPT method. The different irradiances condition representing the different working conditions of PV array are built by the photovoltaic simulator in Fig.11. The dynamic waveforms of I_{PV}, V_{PV}, and P_{PV} with MPPT methods based on PSO and IMA are shown in Fig. 12, the curve of P_{PV} is obtained in a form of the product of I_{pv} and V_{PV}. To obtain fair results, the experimental parameters for PSO and IMA are set as the same.

The fluctuations of V_{PV} and P_{PV} in Fig. 12(a) with PSO-based MPPT method are much bigger than that in

Fig. 12(b) with IMA-based MPPT method, which means that the performance in stability with IMA-based MPPT method is better than that with PSO-based MPPT method. The experimental results are consistent with the simulation results. Moreover, the fluctuating time in Fig. 12(a) is longer than that in Fig. 12(b), which further verify that the dynamic ability of IMA-based MPPT method is better than that of PSO-based MPPT method.

As Fig.13 shows, when the PV system switches from UIC to PSC, where the working states under UIC and PSC are consistent with that in Tab. 2. The tracking time with IMA is about 0.59s, but the tracking time with PSO algorithm is about 1.16s. Compared with PSO-based MPPT method, the IMA-based MPPT method can reduce the tracking time by about 0.57 s. In other words, the IMA MPPT method can increase the tracking efficiency by about 49.1% if the PV system switches from UIC to PSC.

Fig.14 shows the enlarged waveforms of I_{PV}, V_{PV}, and P_{PV} for PSO-based MPPT and IMA-based MPPT methods when the PV system switches from PSC to UIC, where the working states under PSC and UIC are consistent with that in Tab. 2. As Fig.14(a) shows, the tracking time with PSO-based MPPT method is about 1.40s, however, as Fig.14(b) shows, the tracking time with IMA-based MPPT method is about 0.38s. The tracking time with IMA-based MPPT method is shorter about 1.02s than that with PSO-based MPPT method. In other words, the tracking efficiency can be improved by about 72.85% with IMA-based MPPT method compared with PSO-based MPPT method.

The experimental results in Fig.12, Fig.13, and Fig.14 further verify that the performance in convergence time and tracking efficiency of the proposed IMA-based MPPT method are better than that of conventional PSO-based MPPT method, no matter when the PV system switches from PSC to UIC or the PV system switches from UIC to PSC.

VI. CONCLUSION

A MPPT method based on improved mayfly algorithm with shading detection is proposed in this paper. The method can accurately identify the multi-peak situation and single-peak situation of the P-V curve of the PV array under the current irradiance, and adopt different strategies of MPPT control. Moreover, the method can also realize multiple-peak and single-peak MPPT function effectively with elimination strategy and binary search strategy. The simulation and experimental results show that the performance in convergence time, dynamic response, power tracking efficiency and accuracy of the proposed MPPT method based on improved mayfly algorithm are all better than that of the MPPT method based on conventional PSO algorithm.

REFERENCES

[1] N. A. Ludin, N. I. Mustafa, M. M. Hanafiah, M. A. Ibrahim, M. Asri Mat Teridi, S. Sepeai, A. Zaharim, and K. Sopian, "Prospects of life cycle assessment of renewable energy from solar photovoltaic technologies: A review," *Renew. Sustain. Energy Rev.*, vol. 96, pp. 11–28, Nov. 2018.

[2] A. Divya, T. Adish, P. Kaustubh, and P. S. Zade, "Review on recycling of solar modules/panels," *Sol. Energy Mater. Sol. Cells*, vol. 253, May 2023, Art. no. 112151.

[3] V. Jately, B. Azzopardi, J. Joshi, B. Venkateswaran V, A. Sharma, and S. Arora, "Experimental analysis of hill-climbing MPPT algorithms under low irradiance levels," *Renew. Sustain. Energy Rev.*, vol. 150, Oct. 2021, Art. no. 111467.

[4] V. A. M. Lopez, U. Žindžiūtė H. Ziar, M. Zeman, and O. Isabella, "Study on the effect of irradiance variability on the efficiency of the Perturb-and-Observe maximum power point tracking algorithm," *Energies*, vol. 15, no. 20, p. 7562, Oct. 2022.

[5] S. Ngo, T.-D. Ngo, C.-T. Nguyen, and C.-S. Chiu, "A novel approach based incremental conductance method for MPPT strategy of PV systems considering partial shading conditions," *Electric Power Compon. Syst.*, vol. 49, nos. 16–17, pp. 1348–1362, Oct. 2021.

[6] K. Bataineh, "Improved hybrid algorithms-based MPPT algorithm for PV system operating under severe weather conditions," *IET Power Electron.*, vol. 12, no. 4, pp. 703–711, Apr. 2019.

[7] H. Li, D. Yang, W. Su, J. Lü, and X. Yu, "An overall distribution particle swarm optimization MPPT algorithm for photovoltaic system under partial shading," *IEEE Trans. Ind. Electron.*, vol. 66, no. 1, pp. 265–275, Jan. 2019.

[8] N. Pragallapati, T. Sen, and V. Agarwal, "Adaptive velocity PSO for global maximum power control of a PV array under nonuniform irradiation conditions," *IEEE J. Photovolt.*, vol. 7, no. 2, pp. 624–639, Mar. 2017.

[9] D. K. Mathi and R. Chinthamalla, "Enhanced leader adaptive velocity particle swarm optimisation based global maximum power point tracking technique for a PV string under partially shaded conditions," *IET Renew. Power Gener.*, vol. 14, no. 2, pp. 243–253, Feb. 2020.

[10] N. Kumar, I. Hussain, B. Singh, and B. K. Panigrahi, "Rapid MPPT for uniformly and partial shaded PV system by using JayaDE algorithm in highly fluctuating atmospheric conditions," *IEEE Trans. Ind. Informat.*, vol. 13, no. 5, pp. 2406–2416, Oct. 2017.

[11] M. J. Alshareef, "An effective falcon optimization algorithm based MPPT under partial shaded photovoltaic systems," *IEEE Access*, vol. 10, pp. 131345–131360, 2022.

[12] S. Jalali Zand, S. Mobayen, H. Z. Gul, H. Molashahi, M. Nasiri, and A. Fekih, "Optimized fuzzy controller based on cuckoo optimization algorithm for maximum power-point tracking of photovoltaic systems," *IEEE Access*, vol. 10, pp. 71699–71716, 2022.

[13] J.-Y. Shi, D.-Y. Zhang, F. Xue, Y.-J. Li, W. Qiao, W.-J. Yang, Y.-M. Xu, and T. Yang, "Moth-flame optimization-based maximum power point tracking for photovoltaic systems under partial shading conditions," *J. Power Electron.*, vol. 19, no. 5, pp. 1248–1258, 2019.

[14] Y.-P. Huang, M.-Y. Huang, and C.-E. Ye, "A fusion firefly algorithm with simplified propagation for photovoltaic MPPT under partial shading conditions," *IEEE Trans. Sustain. Energy*, vol. 11, no. 4, pp. 2641–2652, Oct. 2020.

[15] R. Sreedhar, P. Chandrasekar, K. Karunanithi, S. C. Vijayakumar, and S. P. Raja, "Design and validation of a single-phase buck–boost inverter with grey wolf optimization algorithm under partial shaded conditions," *Int. J. Inf. Technol.*, vol. 14, no. 7, pp. 3667–3677, May 2022.

[16] J. P. Ram, D. S. Pillai, A. M. Y. M. Ghias, and N. Rajasekar, "Performance enhancement of solar PV systems applying P&O assisted flower pollination algorithm (FPA)," *Sol. Energy*, vol. 199, pp. 214–229, Mar. 2020.

[17] M. Kermadi, Z. Salam, J. Ahmed, and E. M. Berkouk, "A high-performance global maximum power point tracker of PV system for rapidly changing partial shading conditions," *IEEE Trans. Ind. Electron.*, vol. 68, no. 3, pp. 2236–2245, Mar. 2021.

[18] J. Li, Y. Wu, S. Ma, M. Chen, B. Zhang, and B. Jiang, "Analysis of photovoltaic array maximum power point tracking under uniform environment and partial shading condition: A review," *Energy Rep.*, vol. 8, pp. 13235–13252, Nov. 2022.

[19] L. Yi, H. Shi, J. Liu, D. Zhou, X. Liu, and J. Zhu, "Dynamic multi-peak MPPT for photovoltaic power generation under local shadows based on improved mayfly optimization," *J. Electr. Eng. Technol.*, vol. 17, no. 1, pp. 39–50, Jan. 2022.

[20] K. Zervoudakis and S. Tsafarakis, "A mayfly optimization algorithm," *Comput. Ind. Eng.*, vol. 145, Jul. 2020, Art. no. 106559.

[21] K. Ishaque and Z. Salam, "A deterministic particle swarm optimization maximum power point tracker for photovoltaic system under partial shading condition," *IEEE Trans. Ind. Electron.*, vol. 60, no. 8, pp. 3195–3206, Aug. 2013.

HENGSHAN XU was born in Ankang, China, in 1989. He received the B.E. degree from Northwest Agricultural & Forestry University (NWAFU), in 2012, and the Ph.D. degree from North China Electric Power University (NCEPU), in 2018. He is currently with the College of Electrical Engineering & New Energy, China Three Gorges University (CTGU), China. His research interests include active power factor correction, resonant converter, and new energy generation.

MINGYANG ZHAO was born in Chengdu, China, in 1999. He received the B.S. degree in electrical engineering and automation from Southwest Petroleum University (SWPU), Chengdu, in 2021. He is currently pursuing the M.S. degree with China Three Gorges University (CTGU), Yichang, China. His current research interests include maximum power point tracking technology, renewable energy, and the modeling and planning of distribution networks.

FEI XUE was born in Guyuan, China, in 1994. He received the B.S. and M.S. degrees in electrical engineering from Tianjin University, Tianjin, China, in 2014 and 2017, respectively. He is currently an Engineer with the Electric Power Research Institute, State Grid Ningxia Electric Power Company (NEPC), Ningxia, China. His current research interests include maximum power point tracking technology, renewable energy, and the modeling and planning of distribution networks.

XUJUN ZHANG was born in Lanzhou, China, in 1993. He received the B.S. degree in electrical engineering from Lanzhou University, Lanzhou, in 2017, and the M.S. degree in electrical engineering from the Huazhong University of Science and Technology, Wuhan, China, in 2019. He is currently an Engineer with the State Grid Gansu Electric Power Research Institute, Lanzhou. His current research interests include renewable energy and the modeling and planning of distribution networks.

LEIJIE SUN was born in Xuchang, China, in 1989. He received the B.S. degree in electrical engineering and automation from Northwest Agricultural & Forestry University (NWAFU), Xianyang, China, in 2012. He is currently an Engineer with XJ Group Corporation, Xuchang. His current research interests include power system protection, renewable energy, and the modeling of distribution networks.

• • •